2019 International Conference on Robotics and Automation (ICRA)
Palais des congres de Montreal, Montreal, Canada, May 20-24, 2019

A Floating-Piston Hydrostatic Linear Actuator and Remote-Direct-Drive 2-DOF Gripper

Eric Schwarm[1], Kevin M. Gravesmill[1], and John P. Whitney[1,2]

***Abstract*— Dexterous, serial-chain motor-driven robotic arms have high moving mass, since most of the actuators must be located in the arm itself. This necessitates high gear ratios, sacrificing passive compliance, backdrivability, and the capacity for delicate motion. We introduce the concept of a remote direct-drive (RDD) manipulator, in which every motor is located in the base, connected to remote joints via a low-friction hydrostatic transmission. We have designed a new hydrostatic linear actuator with a fully-floating piston; the piston floats within the cylinder using a pair of soft fiber-elastomer rolling-diaphragm seals. This eliminates static friction from seal rubbing and piston/rod misalignment. Actuators were developed with a 20mm bore, weighing 55 grams each with a 400:1 bidirectional strength-to-weight ratio (+/- 230N), which drive a 2-DOF manipulator (wrist pitch/finger pinch; 120-degree range-of-motion; 6.6 Nm max grip strength). The gripper is hydrostatically coupled to remotely-located direct-drive/backdrivable brushless electric motors. System hysteresis and friction are 1 percent of full-range force. This low-mass low-friction configuration is of great interest for powered prosthetic hand design, and passively-safe high dynamic range robot arms.**

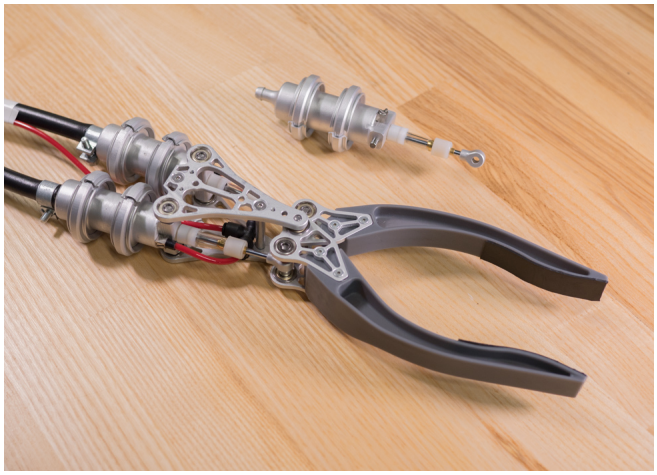

Fig. 1. (color) **(top)** The floating-piston linear hybrid-hydrostatic actuator. **(bottom)** Photograph of the 2-DOF electro-hydrostatic manipulator. Symmetric four bar linkage geometry drives two fingers independently, achieving wrist rotation and grip opening: 120-degree range of motion, 50 N maximum grip force at the fingertip. The gripper shown weighs 220 g.

I. INTRODUCTION

A good, low-cost manipulator would significantly widen the scope of feasible robotics applications. One application is in-home assistive robots for the 15 percent of Americans over the age of 65 suffering from a disability affecting their ability to live independently [1]. The presence of domestic assistive robots in homes is conditional on financial feasibility—unlike the factory setting, in-home robots won't see the rate-of-usage needed to effectively amortize the high cost of an industrial-grade robot. Activities of daily living include feeding, shaving, dressing, cooking, brushing teeth, bathing and opening doors; these tasks require dexterity, precision, and delicate force control, without the luxury of a fully controlled environment. A low-impedance/variable-impedance manipulator that is *also* low cost could make widespread domestic support robots feasible.

A long history of developing low-impedance systems for medical robotics [2], [3] and highly dynamic systems [4], [5], offers insight into the challenges and their possible solutions in this endeavor. A common approach is to develop flexible mechanical transmission systems, such as cable [6], [7] and hydrostatic systems [8]–[10], to reduce the moving mass of an actuator by allowing the driving electric motors to be placed more proximally in the robot, such as in the base of a mobile robot or the ground next to a stationary-base robot. This reduces or eliminates the impact of size and weight constraints of the motors [11], allowing for the selection of more economical components.

Cable driven arms become significantly more complex as the number of degrees of freedom in series increase [4]. In comparison, routing hydraulic lines does not significantly affect the performance of the system and can be routed with less engineering than a cable system.

Pneumatic and hydraulic systems allow very light manipulators due to high torque and power density of fluid actuators. Pneumatic and soft-pneumatic systems can be inexpensive, complaint, and highly adaptable, but they are not suited for high force/position precision tasks due to air compressibility [12], [13] and low bandwidth. Hydraulic systems exhibit high force-bandwidth, but have no passive backdrivability, and are high-cost systems due to precision component machining requirements.

Series-elastic actuation (SEA) [14] adds tuned serial compliance to non-backdrivable actuators; a reduction in force-bandwidth buys enough compliance to provide "active backdrivability" under high-rate closed-loop control. This technique is also interesting for hydrostatic systems, where fluid pressure provides a force feedback signal, and hose volumetric compliance can be tuned to acheive the desired series elasticity.

[1]The authors are with the department of Mechanical and Industrial Engineering, Northeastern University, Boston, MA 02115, USA.
[2]corresponding author, j.whitney@northeastern.edu

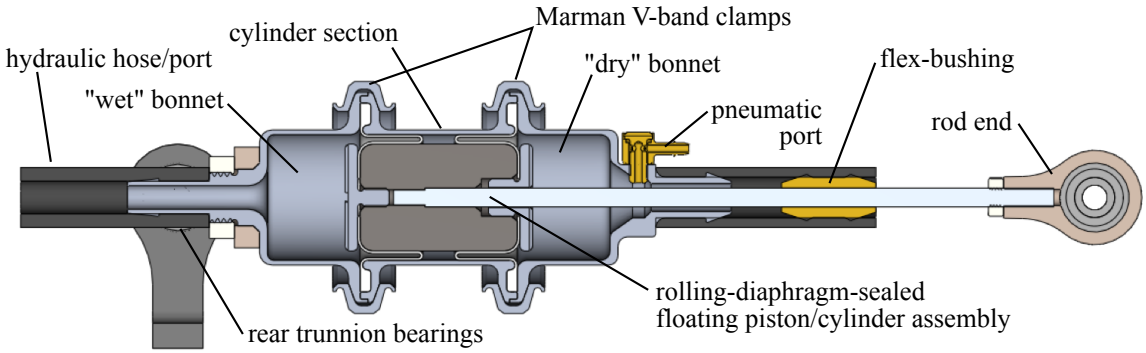

Fig. 2. (color) CAD model section view of the floating-piston/flex-bushing hydrostatic actuator. The wet, hydraulic side is on the left and the dry, pneumatic side is on the right. Ball-bearings (trunnion mount and rod end) along the centerline ensure that there are no net moments placed on the cylinder, eliminating the need for rigid rod support bushings and piston wear rings. Manufactured actuators, including support bearings, weight 55 grams (dry), have a cylinder bore of 20 mm, a 25 mm stroke, and when pneumatically preloaded, a bi-directional maximum force delivery of ± 230 N.

II. HYDRAULIC LINEAR ACTUATOR

Previously developed low-friction rotary hydraulic actuators show promise in developing low-impedance dexterous manipulators [10], but these actuators require an extra timing belt stage to achieve rotary motion, adding friction, and increasing the size of the actuator. Slim linear actuators are better suited for low-profile actuation, particularly for distal degrees of freedom and wrist mechanisms.

The result of the design and manufacturing efforts reported here is a compact, low-friction, low-impedence, hybrid hydraulic and pneumatic linear-stroke actuator. The actuator uses rolling diaphragm seals to convert a pressure difference into a linear force (figure 2).

A. Rolling Diaphragms

Rolling diaphragms are a non-leaking, low-friction alternative to traditional fluid actuator seals. As the piston travels along the stroke, the diaphragm rolls on or off the piston. The diaphragm is sealed along the outer circumference with a molded in o-ring, which is clamped in the flange. Traditional seals compromise between sliding friction and fluid leakage. Fluid leakage is required to lubricate traditional fluid actuators, while the rolling diaphragm seal does not require lubrication.

Rolling diaphragm seals operate at much lower pressures than traditional hydraulic actuators. Low operating pressures are more appropriate for human-interactive systems due to pinhole leakage safety concerns.

B. Marman Band Cylinder Clamps

The cylinder and bonnets are clamped together with Marman clips, which use a V-groove to wedge the flanges together (figure 3). Traditionally, bolted flanges are used to seal diaphragms. The Marman clips eliminate the stress concentration of the flange bolts and replace it with a distributed force around the circumference of the cylinder. The Marman clips are tensioned in place by lockwire located in grooves on each side of the clips. Using a pair of grooves on the shoulder of the clip maintains a low profile, especially compared to the usual technique of using a bolted tab attached to the outside of the V-groove.

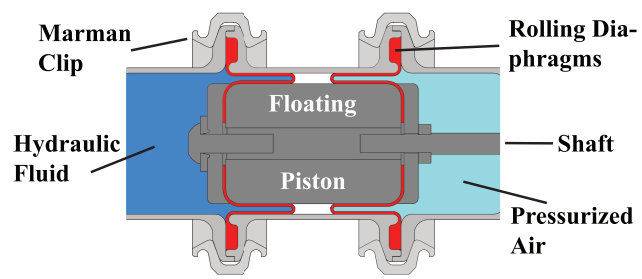

Fig. 3. (color) Diagram of the floating-piston linear hydrostatic actuator, with two Marman V-band clips securing the two cylinder-bonnets to the central cylinder section, and sealing the diaphragm molded-in o-rings. The clips are split into two half-sections, and clamped together by wrapping loops of aviation lockwire around the grooves of marman clips. A 40-degree V-band yields an axial compression force of 8.6-times more than the hoop tension in the band. Diaphragms are Fujikura DM3-20-20; 20mm bore, 24mm stroke, 1.7MPa maximum operating pressure.

C. Hydrostatic Hybrid Hydraulic-Pneumatic Configuration

In a hydrostatic setup, a fixed volume of hydraulic fluid facilitates the force transfer from the master actuator to the slave actuator. A master actuator either compresses the fluid or pulls the fluid, but fluid supports little tension (vacuum) pressure before reaching the vapor pressure of the hydraulic fluid, leading to cavitation. Additionally, rolling diaphragms must maintain a net positive pressure to avoid diaphragm inversion and jamming; the pneumatic preload is used to maintain this positive pressure—allowing bidirectional force and motion transfer without requiring two bulky hydraulic lines per actuator.

A pneumatic preload allows a constant preload force for the full range of motion of the actuator; preload from a linear mechanical spring has variable force; constant force springs and spring-mechanisms are heavy and complex.

D. Floating Piston

A traditional hydraulic cylinder piston is precision ground or lapped to slide inside a hard cylinder wall. Sliding rubber

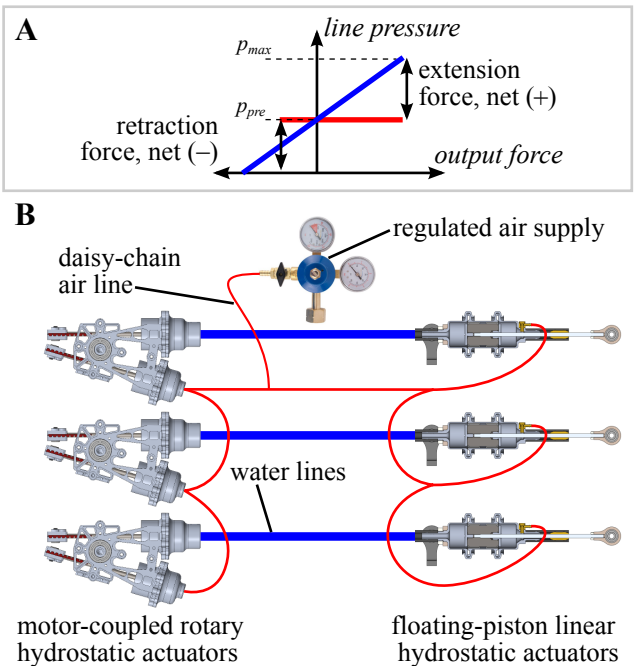

Fig. 4. (color) **(A)** Unidirectional torque capacity is high for light preload, and bidirectional torque capacity is balanced when preloaded to half the maximum pressure rating. **(B)** Multiple rotary hydrostatic actuators are motor driven, and connected to distal linear hydrostatic actuators. Leakage from the shared air line lost to the rod bushings is easy to make up.

seals at each end minimize fluid leakage (although a small amount of leakage is required to maintain seal lubrication), and a pair of wear rings support the piston when subjected to off-axis bending moments, resulting from side loads on the actuator rod.

In contrast, our floating piston design has a rolling diaphragm on each end. The only connection between the piston and the body of the actuator are the two rolling diaphragms, eliminating sliding friction between the piston and cylinder.

In this actuator, the rolling diaphragms at each end of the piston serve a dual role as seal and support. When a side load is present on the piston, via the cylinder rod, the diaphragm is "squished" towards the wall. As the diaphragm is inextensible, this squeezing action causes difference in exposed side area, as shown in figure 5, leading to a restoring force from each diaphragm, F_s, given by

$$F_s = \frac{\pi^2}{8} P D_p \delta, \tag{1}$$

where δ is the piston sideways deflection, D_p is the piston diameter, and P is the fluid pressure.

The axial separation of the diaphragms provides a restoring moment to off-axis loads, resulting in a piston-rod assembly that is self-centering and stable, behaving not unlike a traditional air-bearing.

E. Floating Rod Bushing with Leakage

While the pair of rolling diaphragms do well to seal the hydraulic half of the cylinder and the piston-facing side of

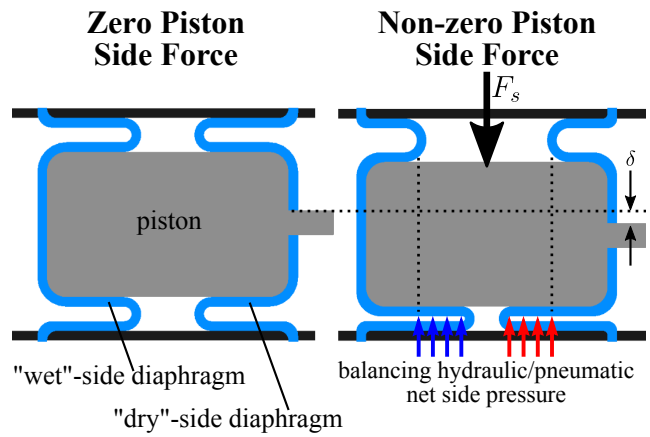

Fig. 5. (color) Illustration of the "air bearing" effect, and self-centering pressure/force response. The independent restoring forces from each diaphragm lead to a force couple that support and stabilize against external moments applied to the piston/rod.

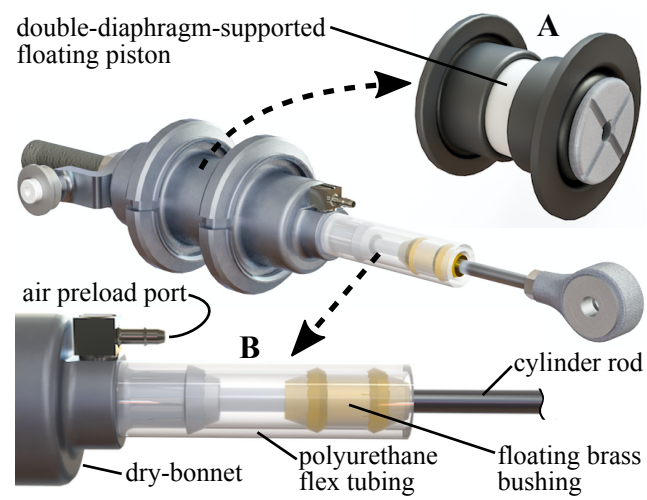

Fig. 6. (color) **(A)** CAD rendering of floating piston supported by two rolling diaphragms. **(B)** The cylinder rod is sealed by a slip-fit brass bushing supported by a section of polyurethane tubing which acts as a flexure mount.

the pneumatic half, an additional seal is required where the cylinder rod must pierce the face of the pneumatic bonnet. Typically a guide bushing is rigidly embedded in the nose of the cylinder, guiding and supporting the rod; *unfortunately, this configuration requires precision alignment of the rod to minimize binding friction, ruining the advantages of rolling-diaphragm seals*. Instead we mount the brass rod bushing (clearance, non-contact fit) in flexible polyurethane tubing, as shown in figure 6, allowing the bushing to shift with the rod, without binding. This is essential to facilitating the self-centering air-bearing effect of the two rolling diaphragms. Assuming fully developed viscous flow within the annular bushing-rod gap, the leak rate, Q, is given by

$$Q = \frac{\pi D A^3 \Delta P}{12 \mu L}, \tag{2}$$

where D is the rod diameter, A is the rod-bushing radial gap, is the internal-external pressure difference, μ is the viscosity

of air, and L is the length of the bushing [15].

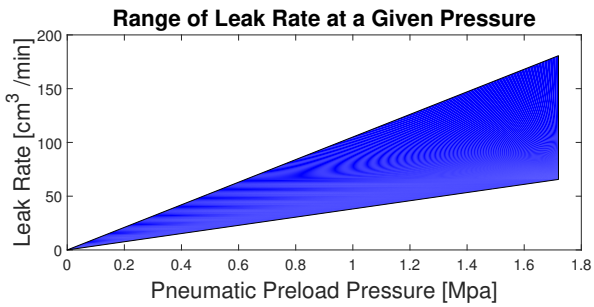

Fig. 7. (color) The leak rate was calculated analytically using equation 2. Bushings are reamed to 10 microns oversize and used without lapping or other advanced fitting technique. Leak rate depends not only on the pressure difference, but diametrical tolerances in the rod (3mm -0.002/-0.008) and bushing.

The leak rate is a function of air preload pressure, and will also vary due to the tolerance variation of the rod. Given manufacturing tolerances, the leak rate for our actuators, shown in figure 7, fall within the shaded blue area for a given pressure in the air side. This leak rate, on the order of 100 cm^3/min, is extremely easy to make up with a tiny air cylinder and regulator.

III. 2-DOF SYMMETRIC FOUR BAR LINKAGE MANIPULATOR

To test the linear hydrostatic actuators, a 2-DOF gripper was designed, offering wrist rotation and finger pinch DOFs (see figures 8 and 9). As both the most distal and most sensitive portion of a manipulator, achieving high grip strength, light weight, and low friction in a gripper is extremely challenging using traditional approaches. Each linear actuator actuates one of the two manipulator fingers. The two fingers are coaxial, allowing them to rotate together (wrist flexion-extension). Each finger has a range of motion of 120 degrees.

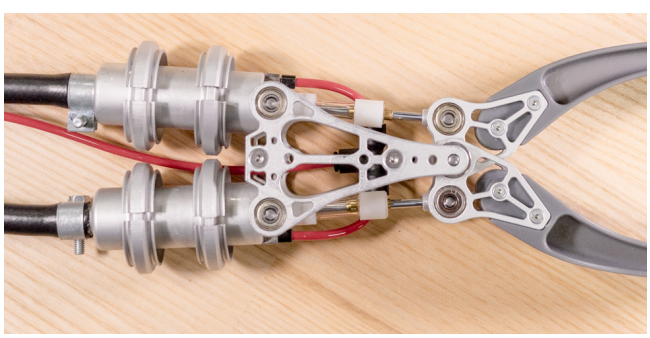

Fig. 8. (color) Close-up side view of gripper. This latest version has mount trunnions on the distal end of the cylinders, facilitating a compact configuration for the side plates. Fingers are removable and modular, attaching to aluminum finger base plates via a wedged joint.

The total mass of the manipulator is 220g. The maximum grip strength is 6.6Nm, or a maximum force of 50N at the fingertips. The grip strength varies with pneumatic preload pressure, as the preload opposes the hydraulic pressure.

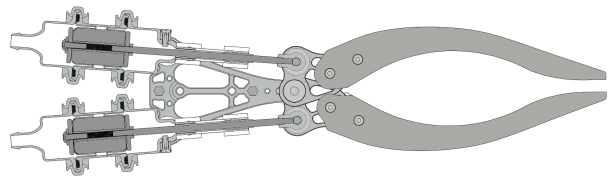

Fig. 9. Cross section diagram of gripper mechanism, highlighting the symmetric 4-bar mechanism and connections between the cylinder rod ends and finger mounting plates.

The manipulator wrist rotation occurs when the linear actuators move opposite each other, one in extension and one in retraction. The manipulator grasp opens when the actuators retract, and closes when they extend.

A. Remote Direct-Drive (RDD) Configuration

The hydrostatically-actuated manipulator offers high torque density and low friction. Were it to be powered using traditional hydraulic flow or pressure valves, the potential for backdrivability and passively-tunable compliance would be lost. Instead, we connect the linear hydrostatic actuators to their rotary cousins, which in turn are connected to large-radius direct drive brushless motors. For these first experiments we are using Akribis ACD120-80 coreless brushless motors, which have zero cogging torque, and a peak torque rating of 6.5 Nm (1.8 Nm continous).

These motors weight 3.2 kg each—making it impossible to use them in the manipulator directly (the RDD hand is, altogether, 30x lighter than it's drive actuators). Figure 4 shows the general plan for remote electro-hyrostatic actuation. The hydraulic lines are preloaded by a single airline connected to the nose-end of every linear actuator, and one end of each proximal rotary actuator. On account of the small air leakage from the linear actuators, a tank of compressed air with a regulator is provided to make-up the leakage.

IV. EXPERIMENTS AND RESULTS

The experimental setup consists of the the 2-DOF gripper hydrostatically coupled to two rotary actuators mounted on electric, direct drive motors as previously discussed. The hydraulic lines are 1.6m long, 6.35mm ID fiber-reinforced rubber. The length, diameter, and radial stiffness of the hose affects the inertia, damping, and stiffness of the transmission.

A. Static Performance

The first experiment demonstrates the stiffness of the system. The gripper is set to close its grasp with maximum PD gains. The fingers are manually separated, then a 5mm thick plate is placed between them. This is repeated with two more 5mm plates to achieve grip openings of 5, 10, and 15mm. Then the plates are removed. Figure 11 shows fingertip force as a function of time, measured via differential hydrostatic pressure. Static stiffness at the fingertips (150mm moment arm) is 300 N/m.

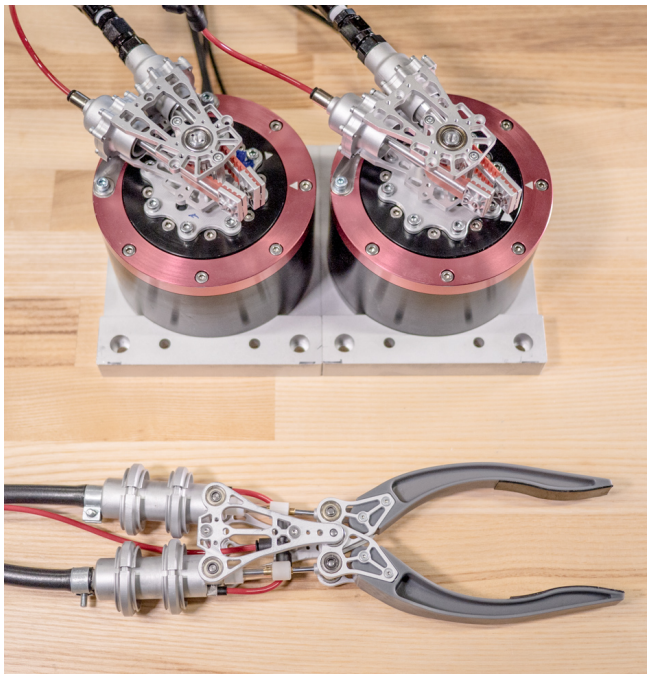

Fig. 10. (color) The experimental setup: the linear actuators in the gripper are coupled to the rotary actuators mounted on direct drive brushless motors, above.

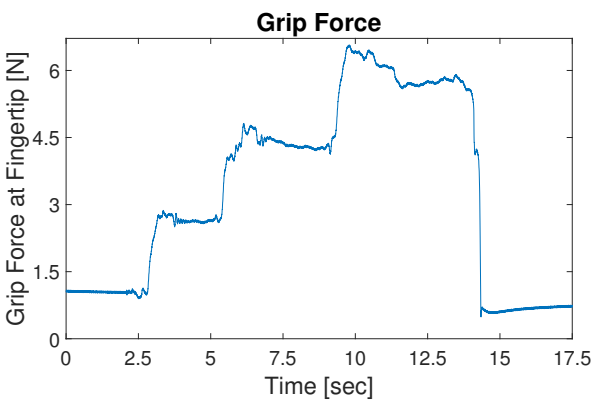

Fig. 11. (color) Result of grasping experiment. Plates with a 5mm thickness were placed between the fingertips. In this plot, there is no gap between the fingertips until 2.5 seconds. From roughly 4 to 5 seconds there is a 5mm gap between the fingertips, then a 10mm gap from 7 to 9 seconds. Finally there is a 15mm gap between the fingertips from 12 to 14 seconds. The spikes in the plot are a result of opening the fingers to place the plates between them.

B. Transparency

The second experiment illustrates the backdrivability of the transmission. The fingers of the gripper were fastened together, with finger backdriving the other with a 0.5 Hz sine wave. The pressure in the driven finger hydraulic and pneumatic lines were measured to determine the backdrive force. Figure 12 illustrates the backdrivability of a gripper finger. The transmission requires approximately 3N of cylinder force (on 230N maximum cylinder force) to backdrive. The experiment was performed with and without the motor attached to the rotary actuator, indicating that motor bearing friction is a larger source of backdrive resistance than the hydrostatic transmission.

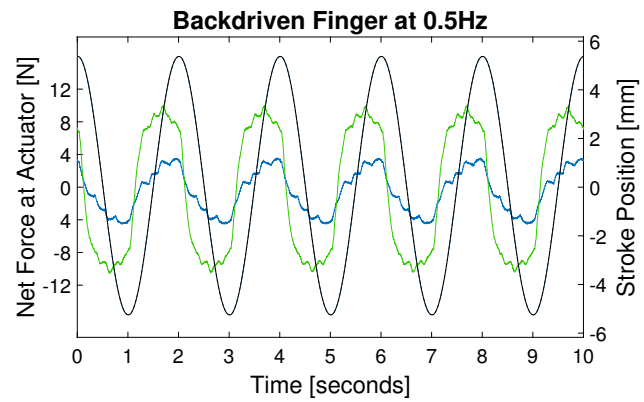

Fig. 12. (color) Result of the backdriving test. The black plot is the stroke position of the driving actuator. The green plot line is the net force in the backdriven finger's linear actuator with the motor attached, while the blue plot line is the net force in the backdriven finger's linear actuator without the motor attached. The difference is a result of the friction and inertia of the motor. The plots are out of phase because the force is a function of velocity and acceleration, not position.

C. Dynamic Performance

Figure 13 shows the response of one finger to a step input (high motor PD gains). The motor provides the step input while fluid pressure is monitored in the hydraulic lines. The response of the fluid pressure indicates a natural frequency (approximate torque bandwidth) of 22 Hz.

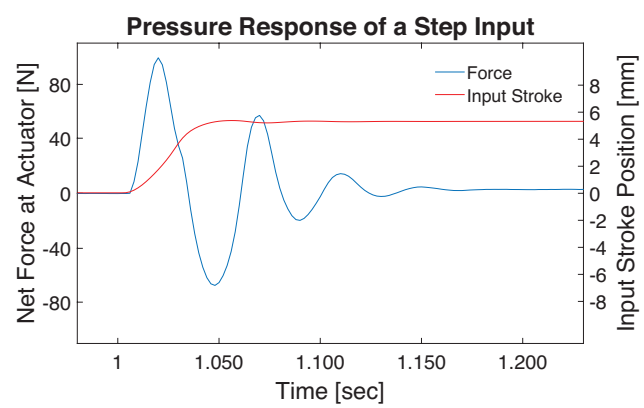

Fig. 13. (color) Step response of one finger. The net force at actuator is the actuator output force resulting from a pressure difference between the hydraulic line and pneumatic preload.

D. Variable Impedance Grasping

All experiments in this paper are performed using pure impedance control; fluid pressures are recorded, but not fed back, and no feedforward terms or hysteresis models are employed.

Figure 14 shows the results from a simple grasping test. A 14mm-wide hex driver is grasped for 5 seconds, and then PD gains are reduced. At $t = 18$ seconds, the motors are turned off. The weight of the hex driver is sufficient to passively

backdrive the lower finger motor and the hex driver falls out of the grasp (see supplemental video for full sequence).

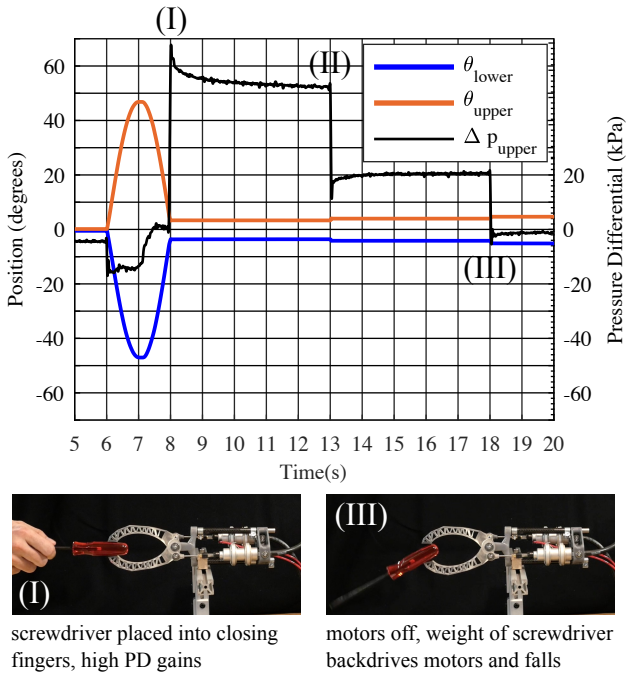

Fig. 14. (color) Result of grasping experiment, in which simple PD control on each finger is used to track half-period sine wave. At $t = 8$ seconds, a hex driver with a 14 mm-wide handle is grasped. At $t = 13$ seconds the PD gains are reduced, and a step-down in measured hydraulic pressure is easily observed. At $t = 18$ seconds, the motors are turned completely off, and the weight of the handle backdrives the motors and falls from the hands grasp, passively.

During the half-period sinusoid, where the fingers are opened up to 90 degrees, and then closed on the object, the total force artifact, including line viscosity, motor friction and inertia, and diaphragm hysteresis, measured via the line fluid pressure, is just 1% of the total force range of the linear actuator. Based on preliminary comparisons between the rotary and linear versions of the hydrostatic transmission, and estimates of motor friction, we expect that using a linear-to-linear transmission, and using low-friction bearings to support the motors (the current motors use large-diameter bearings), will result in an even lower friction/hysteresis artifact, and even better passive backdrivability.

E. Video Supplement

The video supplement to this paper shows manual and motorized grasping and manipulation of objects, and realtime pressure monitoring of the line pressure while grasping objects, and during exposure to very small force perturbations. The low-friction cylinders allow for extremely fine and delicate force resolution via both pressure feedback and motor current monitoring.

V. CONCLUSIONS AND FUTURE WORK

We have developed a new type of hydraulic actuator that fully stabilizes and supports the piston and cylinder without contact seals or contact support bushings. Continuous rolling diaphragm seals eliminate any leakage of hydraulic fluid (water), and a small engineered amount of air leakage at the rod seal (100 cm^3/min) which is inaudible and very easy to makeup—this small leakage pays for the elimination of all rubbing seals and the elimination of nearly all static friction. Additionally, these actuators have been engineered to be very slim and lightweight, offering extremely-high force/work density.

As the rolling-diaphragm sealed actuators have such low static friction, the correlation between hydraulic fluid pressure and output force/torque is nearly perfect. Thus, it is possible to add force feedback/admittance control (e.g. [14]) by simply monitoring fluid pressure. This may be done with inexpensive MEMS pressure sensors, mounted at the proximal end of the transmission, avoiding the added mass of distally-mounted torque sensors and electrical wiring in the arm.

Preliminary tests with remotely-mounted motors driving a 2-DOF wrist/hand manipulator in an electro-hydrostatic configuration show that very delicate and gentle manipulation is possible. The ability of a low-impedance backdrivable system, particularly one with very low friction, to switch instantly from high-gain precision operation to low-gain compliant behavior will enable high-performance autonomous manipulation to succeed when delicate action and precision motion are both required.

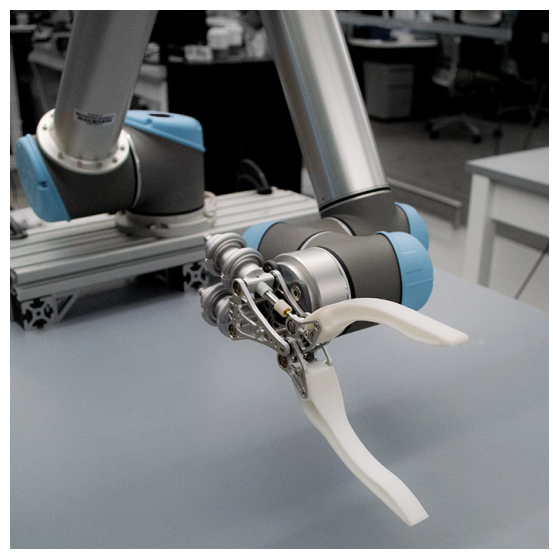

Fig. 15. (color) The 2-DOF gripper installed on the end of a UR-5 robot arm, without hoses attached. The hybrid configuration of stiff, precise proximal joints, with low-impedance distal joints is envisioned as an initial test-bed for investigating learning methods for grasping and manipulation that employ both force and visual feedback.

ACKNOWLEDGMENT

This work is supported in part by the NSF CHS #1617122, #1615891, and NSF NRI 1830425. We thank Xiao Huang and Zikun Yu for assistance on motor control and data collection.

REFERENCES

[1] "A Profile of Older Americans," US Department of Health and Human Services, Tech. Rep., 2015.

[2] A. J. Madhani, G. Niemeyer, and J. K. Salisbury Jr, "The Black Falcon: A teleoperated surgical instrument for minimally invasive surgery," in *Proc. International Conference on Intelligent Robots and Systems*, vol. 2, 1998, pp. 936–944.

[3] S. Charles, H. Das, T. Ohm, C. Boswell, G. Rodriguez, R. Steele, and D. Istrate, "Dexterity-enhanced telerobotic microsurgery," in *Proc. 8th International Conference on Advanced Robotics*. IEEE, 1997, pp. 5–10.

[4] W. T. Townsend and J. K. Salisbury, "Mechanical design for whole-arm manipulation," in *Robots and Biological Systems: Towards a New Bionics?* Springer, 1993, pp. 153–164.

[5] S. Seok, A. Wang, M. Y. Chuah, D. Otten, J. Lang, and S. Kim, "Design principles for highly efficient quadrupeds and implementation on the MIT cheetah robot," in *Proc. International Conference on Robotics and Automation*. IEEE, 2013, pp. 3307–3312.

[6] A. Schiele, P. Letier, R. Van Der Linde, and F. Van Der Helm, "Bowden cable actuator for force-feedback exoskeletons," in *Proc. International Conference on Intelligent Robots and Systems*. IEEE, 2006, pp. 3599–3604.

[7] V. Agrawal, W. J. Peine, and B. Yao, "Modeling of a closed loop cable-conduit transmission system," in *Proc. International Conference on Robotics and Automation*. IEEE, 2008, pp. 3407–3412.

[8] H. Kaminaga, J. Ono, Y. Nakashima, and Y. Nakamura, "Development of backdrivable hydraulic joint mechanism for knee joint of humanoid robots," in *Proc. International Conference on Robotics and Automation*. IEEE, 2009, pp. 1577–1582.

[9] J. P. Whitney, M. F. Glisson, E. L. Brockmeyer, and J. K. Hodgins, "A low-friction passive fluid transmission and fluid-tendon soft actuator," in *Proc. International Conference on Intelligent Robots and Systems*. IEEE, 2014, pp. 2801–2808.

[10] J. P. Whitney, T. Chen, J. Mars, and J. K. Hodgins, "A hybrid hydrostatic transmission and human-safe haptic telepresence robot," in *2016 IEEE International Conference on Robotics and Automation (ICRA)*. IEEE, 2016.

[11] I. W. Hunter, J. M. Hollerbach, and J. Ballantyne, "A comparative analysis of actuator technologies for robotics," *Robotics Review*, vol. 2, 1991.

[12] S. Sanan, M. H. Ornstein, and C. G. Atkeson, "Physical human interaction for an inflatable manipulator," in *Proc. International Conference of the Engineering in Medicine and Biology Society*, 2011, pp. 7401–7404.

[13] N. G. Tsagarakis and D. G. Caldwell, "Development and control of a soft-actuated exoskeleton for use in physiotherapy and training," *Autonomous Robots*, vol. 15, no. 1, pp. 21–33, 2003.

[14] G. A. Pratt and M. M. Williamson, "Series elastic actuators," in *Proc. International Conference on Intelligent Robots and Systems*, vol. 1, 1995, pp. 399–406.

[15] S. P. Buerger, "Stable, high-force, low-impedance robotic actuators for human-interactive machines," Ph.D. dissertation, Massachusetts Institute of Technology, 2005.